Non-alloy Mg anode for Ni-MH batteries

Multiple approaches towards a stable cycling performance

Xu, Yaolin; Mulder, Fokko M.

DOI
10.1016/j.ijhydene.2021.03.073

Publication date
2021

Document Version
Final published version

Published in
International Journal of Hydrogen Energy

Available online at www.sciencedirect.com

ScienceDirect

journal homepage: www.elsevier.com/locate/he

Non-alloy Mg anode for Ni-MH batteries: Multiple approaches towards a stable cycling performance

Yaolin Xu [1], *Fokko M. Mulder* [*]

Materials for Energy Conversion and Storage (MECS), Department of Chemical Engineering, Faculty of Applied Science, Delft University of Technology, Van der Maasweg 9, Delft, 2629, the Netherlands

HIGHLIGHTS

- Non-alloy Mg has been for the first time utilized as anode in Ni-MH batteries.
- TiF_3 catalyzed Mg achieves reversible H sorption to $MgH_{0.13}$ at room temperature.
- Nickel foil prevents the passivation of Mg while allows for H permeation.
- NaOH/KOH eutectic at 200 °C works effectively as electrolyte for Ni-MH batteries.
- [SET3][TFSI] ionic liquid and PVA-NaOH/KOH membrane are tested as electrolyte.

GRAPHICAL ABSTRACT

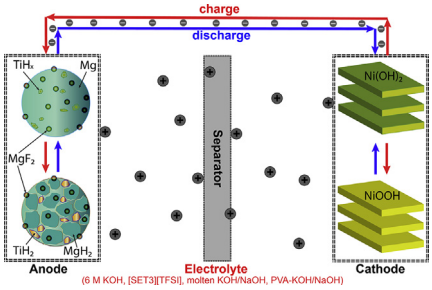

ARTICLE INFO

Article history:
Received 29 September 2020
Received in revised form
15 February 2021
Accepted 9 March 2021
Available online 23 April 2021

Keywords:
Ni-MH batteries
Electrochemical hydrogen storage
MgH_2
Encapsulation
Ionic liquid
Alkaline polymer membrane

ABSTRACT

Mg attracts much research interest as anode material for Ni-MH batteries thanks to its lightweight, cost-effectiveness and high theoretical capacity (2200 mA h g^{-1}). However, its practical application is tremendously challenged by the poor hydrogen sorption kinetics, passivation from aggressive aqueous electrolytes, and insulating nature of MgH_2. Mg-based alloys exhibit enhanced hydrogen sorption kinetics and electrical conductivity, but significant amount of costly transition metal elements are required. In this work, we have, for the first time, utilized non-alloyed but catalyzed Mg as anode for Ni-MH batteries. 5 mol.% TiF_3 was added to nanosized Mg for accelerating the hydrogen sorption kinetics. Several strategies for preventing the problematic passivation of Mg have been studied, including protective encapsulation of the electrode and utilizing room-temperature/high-temperature ionic liquids and an alkaline polymer membrane as working electrolyte. Promising electrochemical performance has been achieved in this Mg–TiF_3 composite anode based Ni-MH batteries with room for further improvements.

* *Corresponding author.*
E-mail address: F.M.Mulder@tudelft.nl (F.M. Mulder).
[1] Present address: Department of Electrochemical Energy Storage (EM-AEES), Helmholtz-Zentrum Berlin für Materialien und Energie, Hahn-Meitner-Platz 1, 14,109 Berlin, Germany.

https://doi.org/10.1016/j.ijhydene.2021.03.073

Introduction

Due to its long cycle life, high energy density and safety, Ni-MH batteries have been one of the most important power sources for various applications [1–3]. The commercially available Ni-MH battery consists of a $Ni(OH)_2$ cathode and $MmNi_5$ (Mm: mishmetal, an alloy of rare-earth elements; and Ni is often partially replaced by Co and Al.) anode separated by an aqueous alkaline electrolyte wetted separator, and has a reversible capacity of about 300 mA h g^{-1} [4]. The main reactions involved in a Ni-MH battery are shown below, resulting in a nominal operating voltage of about 1.25 V at room temperature (RT) (Fig. S1 in the Supplementary Information (SI)).

$$\text{Cathode: } Ni(OH)_2 + OH^- = NiOOH + H_2O + e^- \quad (1)$$

$$\text{Anode: } M + nH_2O + ne^- = MH_n + nOH^- \text{ (M: hydrogen storage metal/alloy)} \quad (2)$$

However, the high cost and the limited capacity of rare-earth materials based anodes has significantly compromised its advantages over other rechargeable batteries, such as the nowadays commercial Li-ion batteries [5,6]. Extensive efforts have been dedicated in the search of new metal hydride candidates for Ni-MH batteries, among which the MgH_2 has attracted intensive research interest in recent years because of its light weight, abundance and high theoretical capacity for hydrogen storage (2200 mA h g^{-1}) [7–14]. However, its practical realization in Ni-MH batteries suffers from three major plagues. (i), The hydrogen desorption kinetics of MgH_2 is slow due to its high thermodynamic stability and thus high energy required for hydrogen dissociation. (ii), The MgH_2 that is formed during charge is electronically insulating. (iii), Mg, upon contact with aqueous electrolytes, reacts with H_2O instantaneously creating a passivation $Mg(OH)_2$ layer which prevents the desired reactions to occur and consumes the active materials, and this issue becomes aggravated over cycling induced by the pulverization of active materials creating fresh surface exposed to the aggressive electrolyte.

To enhance the hydrogen sorption kinetics to enable reaction at room temperature, metastable Mg-based alloys, especially Mg–Ni alloys, have been intensively researched [15–35] as alternative to pure Mg working as the anode for Ni-MH batteries. In these alloys, large amount of transition metals (e.g. Ni, Ti, Ce, Sc, Pd, etc.) are alloyed with Mg to destabilize the Mg–H system to accelerate the hydrogen sorption kinetics and to enhance conductivity of the hydride. For example, an anode of $Mg_{0.9}Ti_{0.1}Ni_{0.95}Pd_{0.05}$ alloy mixed with Cu powder achieved a capacity retention of 192.2 mA h g^{-1} in 20 cycles [15]. $Mg_{0.7}Ti_{0.3}Ni_{1.0}$ alloy delivered an initial capacity of 325 mA h g^{-1}, and 92% of which could be retained after 20 cycles [16]. 20 h ball-milled $Mg_{50-x}Ti_xNi_{45}Al_3Co_2$ achieved capacities from 405.0 to 519.4 mA h g^{-1} with a capacity retention rate from 45% to 72% after 100 cycles [17]. Ball-milled $Mg_{1-x}Ce_xNi_{0.9}Al_{0.1}$ (x = 0–0.08) + 50 wt% Ni alloy reached capacities ranging from 352.6 to 536.9 mA h g^{-1} when varying the content of Ce and the milling duration [18]. Meanwhile, Mg-X (X: Ti, Sc, V and Cr) thin films can reach up to six times of the capacity of the commercial Ni-MH battery [19–21]. However, surface modifications of these Mg alloys are necessary to avoid the surface passivation. For instance, Pd coating was implemented, which not only enhances the hydrogen uptake/release properties but also protects Mg from the aggressive electrolyte. Rongeat et al. reported that the cycle life of a MgNi anode can be slightly improved by surface modification with electroless deposition of chromate or coating of TiO_2 [26]. Anodes of Mg–Ni alloy thin films also showed improved cycle life for Ni-MH batteries through surface coating of $MmNi_5$ [27]. Overall, despite the progress that has been achieved for Mg-based alloys in electrochemical hydrogen storage, their capacities are still much lower compared to pure Mg, not to mention that the cost of these transition and noble metals like Sc and Pd is high, and the commercial viability of the surface encapsulation methods is also limited. It is also noted that no pure (i.e., non-alloyed) Mg has been explored in Ni-MH batteries.

Moreover, transition metal compounds, such as metal halides, have demonstrated significant catalytic effect on the hydrogen sorption kinetics of MgH_2 [36–40]. Our previous studies [41–43] also showed that, in gas phase hydrogen sorption experiments and electrochemical cells, by nanosizing and adding catalyst like TiF_3 the hydrogen sorption kinetics in Mg can be significantly facilitated. Interesting to note is also that the nanostructure is preserved upon cycling by the seed crystal like grain refinement functioning of the added catalyst. Therefore, the nanostructured Mg–TiF_3 composite appears to be attractive as an anode for Ni-MH batteries, and we have, in this work, investigated the electrochemical performance of nanosized Mg catalyzed with 5 mol. % of TiF_3 working as an anode in full-cell Ni-MH batteries. Based on the catalytic mechanism of TiF_3 we proposed in Refs. [41,42], a schematic of the Ni-MH battery with a $Ni(OH)_2$ cathode and a Mg–TiF_3 anode is illustrated in Fig. 1. The titanium hydride is a metallic conductor, in contract with MgH_2, which potentially aids in the electron transport.

To achieve a stable electrochemical cycling performance, we have studied several approaches to prevent Mg from aggressive passivation from aqueous electrolyte in this work, as described below.

(1) Encapsulation of the Mg electrode with nickel foil (NF) when an aqueous alkaline electrolyte is used. The NF works as a protection against the aggressive electrolyte while allowing for the permeation of H [44,45]. Though gas-phase hydrogen diffusion in nickel is slow,

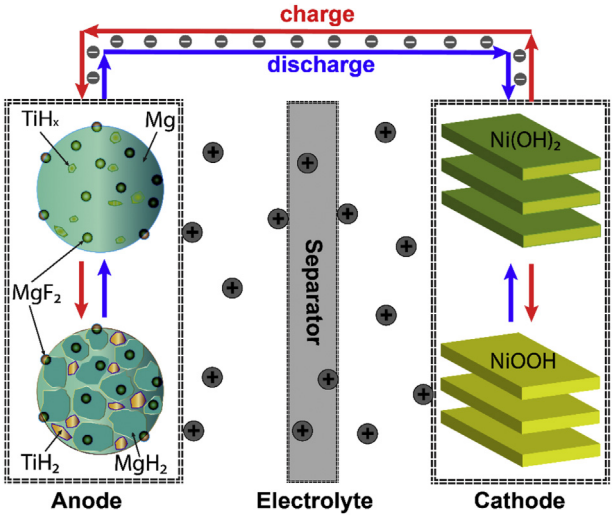

Fig. 1 – A schematic of the Ni-MH battery with a $Ni(OH)_2$ cathode and an anode based on TiF_3 catalyzed Mg.

we expected that electrochemical hydrogen permeation through nickel may be significantly enhanced, due to the presence of an applied electrical field as driving force for hydrogen insertion in nickel.

(2) For non-protected Mg anode, non-aggressive electrolytes, in which Mg exhibits high chemical stability and thus the passivation issue is eliminated, have been introduced.

(2a) RT ionic liquid (IL) electrolyte: Triethylsulfonium bis(-trifluoromethylsulfonyl)imide ([SET3][TFSI])

The properties of IL, such as high thermal and electrochemical stability, relatively high ionic conductivity and low vapor pressure, make it ideal for various electrochemical applications. RT ILs have been investigated as electrolytes in energy storage applications such as lithium ion batteries [46] and fuel cells [47]. An RT IL based electrolyte (1-ethyl-3-methylimidazolium acetate ([EMIM][Ac]) mixed with glacial acetic acid) has recently been investigated in Ni-MH batteries as an alternative to the conventional aqueous KOH electrolyte [48]. In this work, we investigated a RT IL, [SET3][TFSI], which has a relatively high ionic conductivity and electrochemical stability [49] and has been used as the electrolyte in supercapacitors [50,51], as the working electrolyte for the Mg anode based Ni-MH batteries to avoid the passivation issues.

(2b) High temperature (HT) IL electrolyte: molten NaOH/KOH working at 200 °C.

We were intrigued by the NaOH/KOH eutectic electrolyte that exhibits a reduced melting point at 170 °C (compared to > 300 °C for either of these two hydroxides) and has been applied in ammonia fuel cells [52] and ammonia synthesis [53]. In this work, we introduced this molten hydroxide electrolyte to Ni-MH batteries as the working electrolyte.

(2c) RT anhydrous alkaline polymer electrolyte: polyvinyl alcohol (PVA) - NaOH/KOH.

Alkaline polymer electrolytes exhibits advantages such as limited corrosivity compared to conventional aqueous alkaline electrolytes, high ionic conductivity, electrochemical stability and mechanical flexibility, and thus have received much research attention to be used as the electrolyte in Mg based Ni-MH batteries [54–56]. However, despite the improvement compared to an aqueous KOH electrolyte, the alkaline polymer membranes in the these reports were not anhydrous and the Mg based anodes still got passivated by OH^- and the cycling performance was poor. For instance, a PVA-polyacrylic acid (PAA)-KOH polymer electrolyte was reported to exhibit a high ionic conductivity of 0.019 S cm^{-1} at room temperature, however, the Mg_2NiH_4 anode got passivated during cycling, resulting in a poor cycling performance (retained capacity in 10 cycles: 14.7% of the initial cycle) [54]. An anhydrous alkaline polymer membrane exhibits advantages over the conventional alkaline polymer electrolytes, such as light weight and non-corrosivity. Therefore, we have investigated the possibility of an anhydrous alkaline polymer membrane, PVA-NaOH/KOH, functioning as the electrolyte for Mg anodes based Ni-MH batteries.

In brief, this is, for the first time, non-alloyed but catalyzed Mg has been utilized as an anode material for Ni-MH batteries. The catalysis of TiF_3 enables a reversible hydrogen sorption in the nanosized hexagonal Mg metal phase to a certain concentration (up to $MgH_{0.13}$) at room temperature. The passivation of the Mg anode has been effectively mitigated through simple encapsulation or using an IL electrolyte, enabling reversible electrochemical hydrogen storage in Mg with room for further improvement.

Experimental details

Sample preparation

Anode materials

The anode material in this work is a Mg–TiF_3–Ni composite produced from dehydrogenation of a MgH_2–TiF_3–Ni mixture. The catalytic TiF_3 is added to enhance the hydrogen sorption kinetics, and Ni powder is applied to improve the electronic conductivity of the electrode. The sample was prepared in following steps: Firstly, MgH_2 (Alfa Aesar, > 98%) and TiF_3 (Alfa Aesar, > 99.9%) powders were heated in an Ar-environment glovebox with the O_2 and H_2O levels < 0.1 ppm to remove any remaining volatile impurities, at 150 °C and 250 °C, respectively for 2 h. Then the mixture of MgH_2 with 5 mol. % TiF_3 was ball milled under Ar atmosphere using a Fritsch Pulverisette 6 planetary monomill with a rotational speed of 400 rpm for 2 h, and the ball-to-powder mas ratio was 50 : 1. To eliminate the excess heat generated from mechanical milling that may cause the dehydrogenation of MgH_2, the milling period was divided into 8 repetitions of a 15-min milling followed with a 15-min rest to allow the grinding bowl to cool down in between. Subsequently, 5 wt % Ni nano powder (<100 nm, Sigma Aldrich) was added to the ball miled MgH_2–TiF_3 and mixed uniformly by further ball milling the MgH_2–TiF_3–Ni mixture at 100 rpm for 30 min. Finally, the ball milled MgH_2–TiF_3–Ni sample was gradually dehydrogenated to Mg–TiF_3–Ni inside an Ar-filled glovebox between RT and 300 °C within 3 h: 150 °C for the 1st hour, 250 °C during the 2nd h and 300 °C in

the last hour. The completely dehydrogenated Mg–TiF_3–Ni composite is denoted as MTN in this article.

Cathode

The cathode (active material: $Ni(OH)_2$) was obtained directly from fully discharged and then disassembled commercial rechargeable Ni-MH batteries (GP Recyko, 2050 mA h), and was dried at 100 °C to remove the water content and stored in an Ar environment glovebox.

Sample characterization

X-ray diffraction (XRD) was performed with a PANalytical X'Pert Pro PW3040/60 diffractometer with Cu K_α radiation working at 45 kV and 40 mA. A lab-designed airtight sample holder with a Kapton® window was used to protect the specimen from any oxidation. Scanning electron microscopy (SEM) images were obtained with a JEOL JSM 6010F scanning electron microscope that operates with an accelerating voltage of 10 kV.

Fabrication of electrochemical cells

Electrochemical cells with a RT aqueous electrolyte

For the Ni-MH batteries working with aqueous electrolytes, a 6 M KOH water based solution was applied as the working electrolyte. The electrodes were prepared in the following process: Firstly, an MTN pellet was obtained by pressing the MTN powder into a pellet (7 mm in diameter) with a die set and a hand press. Subsequently, to prevent corrosion from the aqueous electrolyte, one side of the reactive Mg electrode was covered with a thin NF (15 mm in diameter; 20 μm in thickness) which is transparent for protons but isolates the electrode from the aggressive aqueous electrolyte. The lateral and the other side of the pellet was coated with a thin layer of Ag paint (SPI Supplies) in order to improve the electronic conductivity and at the meantime achieving the entire cladding of the Mg electrode. The final configuration of the electrode is an MTN pellet completely enfolded by Ag coating and NF with only the NF side accessible for hydrogen transport.

Swagelok cells with a stainless steel (SS) body and two SS caps (Fig. S2a–S2d) were used and the batteries were assembled inside an Ar-environment glovebox. To assemble the batteries, one Ag-MTN-NF electrode was put onto one SS cap and then a glass micro fibre separator wetted with electrolyte and a piece of $Ni(OH)_2$ cathode, respectively in turn, were placed on top and finally the cell was closed with the other SS cap. It should be noted that the Mg electrode was placed with the NF side facing towards the electrolyte.

Electrochemical cells using a RT IL electrolyte

The RT IL, [SET3][TFSI] (Fluka), was employed in this work to replace the aqueous electrolyte in order to avoid the passivation issues. A pressed pellet of MTN without protections was utilized as the anode and the commercial $Ni(OH)_2$ cathode worked as the counter electrode. The cell was the same Swagelok cell working with an aqueous electrolyte.

Electrochemical cells working with a HT IL electrolyte

The HT IL, molten NaOH/KOH (1:1 in mole), was applied as the working electrolyte operating at 200 °C for Ni-MH batteries. Prior to electrolyte preparation, KOH and NaOH were dried at 100 °C for a week inside the glovebox. The electrochemical cell was a similar Swagelok cell but with a Teflon temperature-resistant body (Fig. S2e–S2h), and assembled with the same procedures as described above. All components of the cell were kept at the working temperature while the battery was assembled to prevent the solidification of the eutectic electrolyte.

Electrochemical cell with a RT alkaline polymer electrolyte

In the Ni-MH batteries that worked with PVA-NaOH/KOH electrolytes (preparation details in the SI), the polymer membrane served as both an electrolyte and a separator. The working electrodes were an anode of pressed MTN pellet (without Ag/Ni capping) and a commercial $Ni(OH)_2$ cathode, respectively; and the electrochemical cell was the same Swagelok cell as the one used for the aqueous/RT IL electrolyte.

Electrochemistry measurement

The galvanostatic/potentiostatic electrochemical properties of the batteries were tested with a MACCOR 4600 battery cycler. To protect the Mg based electrode from any possible gas/moisture invasion from the ambient environment, the cells were placed inside an Ar-filled glovebox during charge and discharge. The cells working with the aqueous KOH, [SET3][TFSI] and PVA-NaOH/KOH electrolytes were tested at RT; while the cells working with a molten NaOH/KOH electrolyte were kept at a constant temperature of 200 °C with a heating system.

Results and discussions

Characterization

The samples before and after hydrogen desorption were characterized with XRD and SEM as shown in Fig. 2. XRD patterns (Fig. 2a) of the ball milled MgH_2–TiF_3–Ni show characteristic peaks of β-MgH_2 together with the presence of a small portion of γ-MgH_2; peaks corresponding to TiF_3 and nickel are also observed. After hydrogen desorption, both β- and γ-MgH_2 disappear while the peaks of Mg emerge, which confirms the complete dehydrogenation of MgH_2 (**Reaction (3)**). Meanwhile, nickel remains and TiF_3 converts in reaction with MgH_2 as the peaks of MgF_2 and TiH_x arise, indicating the occurrence of **Reaction (4)**. These observations are in good agreement with our previous report [42]. In addition, peaks at 42.9° and 62.0° in the XRD patterns of the non-desorbed sample can be assigned to MgO revealing the presence of an unavoidable native oxidation layer. The MgO has been partly reduced to metallic Mg by the released hot H_2 gas from MgH_2 during the hydrogen desorption process as the MgO peaks have been significantly reduced in the desorbed sample.

$$MgH_2 \rightarrow Mg + H_2 \uparrow \quad (3)$$

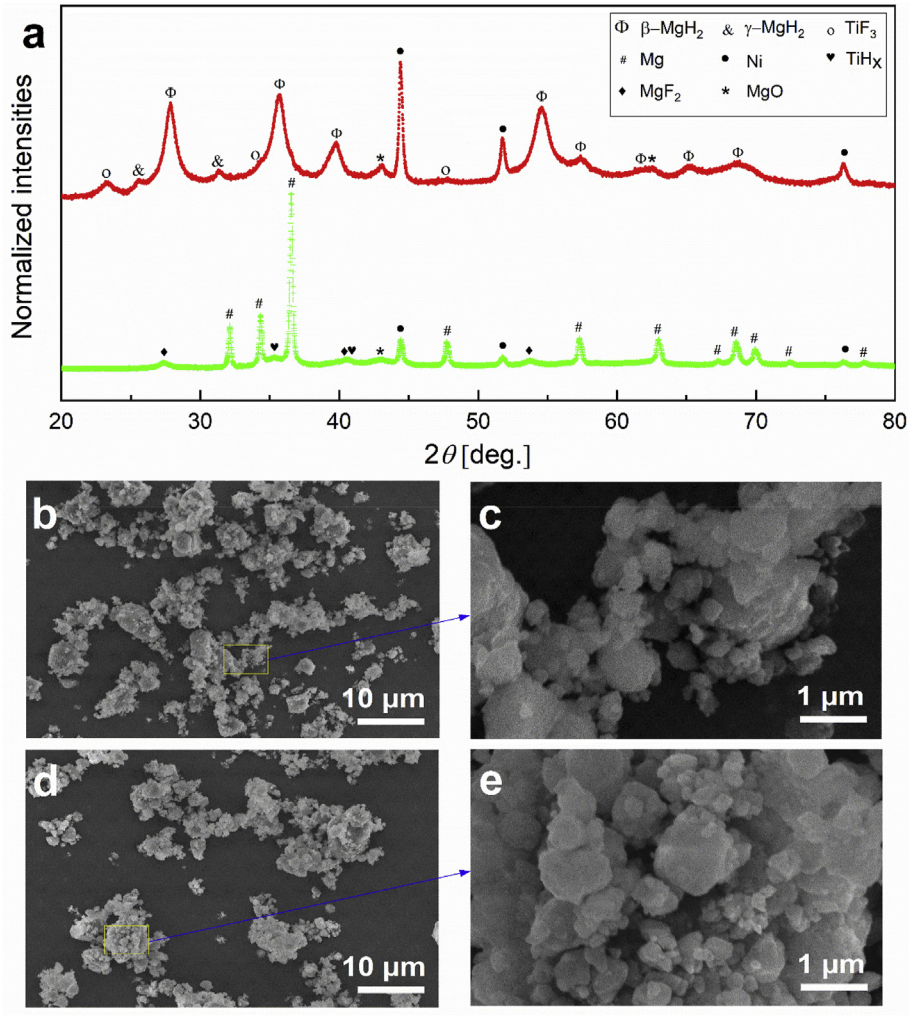

Fig. 2 – Characterization on the samples. (a), XRD patterns and micro-morphologies of the MTN sample before ((b)–(c)) and after ((d)–(e)) hydrogen desorption.

$$3\,MgH_2 + 2\,TiF_3 \rightarrow 3\,MgF_2 + 2\,TiH_x + (3\text{-}x)\,H_2 \uparrow \quad (4)$$

The ball-milled MgH_2–TiF_3–Ni sample appears as micro scale agglomerations of submicro-/nanosized grains as observed in the micrographs (Fig. 2b and c); and after dehydrogenation, the MTN sample shows a similar morphology (Fig. 2d and e). Rietveld refinement on the XRD patterns (Fig. S3–S4 & Table S1–S2) reports that the average crystalline domain size of MgH_2 and TiF_3 is 7.8 nm and 5.0 nm, respectively, indicating that the materials have been nanosized through the mechanical ball milling. After hydrogen desorption the size of Mg appearsto be ~75 nm. This is due to the fusion of Mg nano-domains during the heat induced dehydrogenation process; however, it is important to note that the crystallites are still nanosized and not grown to micron size thanks to the grain refinement action of the MgF_2 and TiH_x [42,57]. The size of MgF_2/TiH_x is small (~10 nm) which results in numerous catalytic sites and high catalyzing activity and thus guarantees a maximum catalytic effect for hydrogen sorption.

Electrochemical performances

Aqueous electrolyte

The Ni-MH battery working with an aqueous electrolyte exhibits a cell configuration of Ag-MTN-NF ‖ 6 M KOH (aq.) ‖ $Ni(OH)_2$. The NF is utilized as a protective layer, which works as a permselective layer for protons plus electrons but physically separates the reactive Mg/MgH_2 from the aqueous electrolyte and thus prevents the aggressive corrosion. It should be noted that nickel itself does not stay hydrogenated (Fig. S5), and the permeability of hydrogen through NF has been validated but with limited kinetics (Fig. S6). Meanwhile, the NF's efficacy of protection is limited, resulting in leakage spots for alkaline electrolyte (Fig. S7), where proton diffusion in aqueous electrolyte would also take place during cycling.

During charge, water electrolysis can occur when the voltage reaches >1.23 V, and the electrolyte solvent will be irreversibly split into gaseous H_2 and O_2, which largely compromises the Coulombic efficiency (ratio of the discharge to charge capacity) and consumes the electrolyte. Therefore, to improve the Coulombic efficiency the battery was charged at a constant voltage of 1.5 V, limiting the unwanted electrolyte

loss. With the potentiostatic charge mode the current response is expected to be high initially and decreases exponentially over time [58], and thus most of the capacity would be achieved during the very beginning stage while the water splitting would be limited as the high current rate would bring the practical electrolysis voltage way above the operating voltage (1.5 V) [59]; meanwhile, the current rate would remain extremely low during most of the charge period during which more capacity would be gained slowly.

Fig. 3a shows that the maximum charge capacity reaches 146 mA h g^{-1} which can be recalculated to $MgH_{0.13}$ when taking into account of the theoretical capacity of 2200 mA h g^{-1} for MgH_2, and the discharge capacity is around 110 mA h g^{-1} (i.e. $MgH_{0.10}$). It is observed in Fig. 3b that during the potentiostatic charge, as expected, an extremely high current response (>3000 mA g^{-1}) occurs at the initial stage (fast charge); whereas the long tail of the current curve (lasting for more than 9.5 h, slow charge) exhibits a low current rate of only about 4 mA g^{-1}. Therefore, most of the capacity has been achieved in the very initial stage (nearly 50% of total charge capacity has been reached even within the first 5 min)

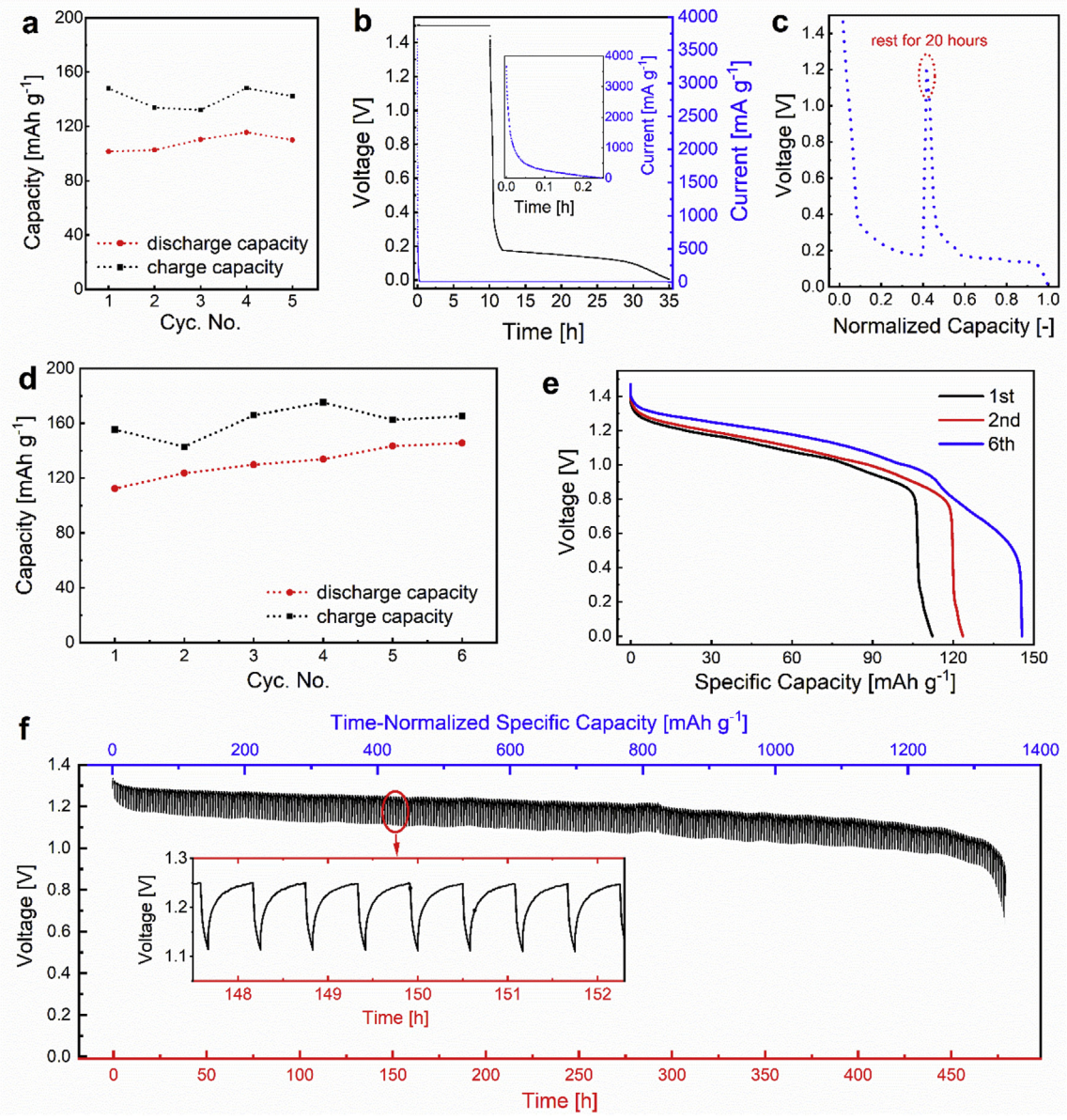

Fig. 3 – Electrochemical performance of the battery: Ag-MTN-NF || 6 M KOH (aq.) || $Ni(OH)_2$ working at RT (mass loading of Mg in (a)–(c): 36.6 mg cm^{-2}, (d)–(e): 9.2 mg cm^{-2} and (f): 8.4 mg cm^{-2}). In (a)–(e), potentiostatic charge at 1.5 V was applied with a fixed time of 10 h and the discharge was stopped when the voltage reached 0 V. The discharge rate is 4 mA g^{-1} in Fig. (a)–(c) and 0.5 mA g^{-1} in Fig. (d)–(e). Fig. (f) shows the GITT discharge voltage profile: discharge at 20 mA g^{-1} for 5 min followed with a rest period of 30 min. The x-axis is scaled in time [h] as well as in the time-normalized specific capacity [mAh g^{-1}]. The battery was charged at 110 mA g^{-1} for 20 h before it was discharged with a GITT mode (galvanostatic charge voltage profile prior to the GITT-discharge in Fig. S8).

The fast charge part can be compared to the fast loaded hydrogen in gas phase. It was confirmed by some of us using neutron diffraction that up to 25% of total hydrogen capacity can loaded to Mg metal in a very short time before β-MgH_2 phase starts nucleation and growth [41]. Therefore it is suggested that the quickly electrochemically loaded hydrogen also results in a solid solution phase in the hexagonal α-Mg phase. Once the stable hydride phase starts forming the previously conductive α-Mg becomes insulating β-MgH_2 which reduces the electronic conductivity, and the electrochemical performance deteriorates. The achieved hydrogenation capacity ($MgH_{0.10}$) is consistent with our previous report that the enthalpy of formation for the MgH_x-TiF_3 compound loaded up to a concentration of $x = 0.14$ is around - 46 kJ mol^{-1} which fits in the range of the enthalpies that guarantees a reversible hydrogen uptake at a pressure between 0 and 5 bar and a temperature up to 45 °C [57,60].

When the battery is discharged at 4 mA g^{-1}, a discharge plateau appears at ~0.15 V (Fig. 3b), which is much lower than the theoretical operating voltage (1.25 V). It may be the result of a significant overpotential and is confirmed by the voltage rise to 1.19 V after a relaxation period of 20 h at the halfway of the discharge plateau (Fig. 3c). The high overpotential is probably contributed by two main factors: the reduced hydrogen transport kinetics due to the presence of NF, and the limited hydrogen diffusion in the thick, non-porous electrode solid. Meanwhile, the Coulombic efficiency at max. 83% is less than 100%, in which the sluggish kinetics of hydrogen desorption may play a major role (as the water splitting has already been suppressed).

To minimize the overpotential and to improve the kinetically limiting discharge capacity, an electrode that is four times thinner was tested at a lower discharge current rate of 0.5 mA g^{-1} and the electrochemical performance is shown in Fig. 3d and e. It is observed that the discharge voltage shows a plateau at ~1.2 V, indicating a negligible overpotential attributed to a facilitated hydrogen diffusion matched with the current flow. Moreover, the voltage plateau rises slightly and the discharge capacity also grows over cycling, indicating the Mg–TiF_3 electrode undergoes an activation process for reversible hydrogen uptake. The initial discharge capacity is 112 mA h g^{-1}, and it goes up gradually to 145 mA h g^{-1} in 6 cycles which corresponds to a hydrogen concentration of $MgH_{0.13}$. In addition, it should be noticed that the Coulombic efficiency of the Ni-MH battery has been promoted (up to 88%) but is still to be improved.

In the above discussions, the charge (hydrogenation) capacity is far away from the theoretical capacity and is mainly limited by the achieved capacity during the initial fast charge process, and thus the following discharge capacity is limited (by the charge capacity). Therefore, the potentiostatic charge at 1.5 V is not appropriate when a high capacity or even the theoretical value is targeted. To explore the maximum reversible capacity of the MTN electrode and to obtain the equilibrium potential of dehydrogenation, the battery was charged with a galvanostatic mode at 110 mA g^{-1} to the theoretical capacity (2200 mA h g^{-1}, Fig. S8) and discharged with a galvanostatic intermittent titration technique (GITT) mode. During discharge, it shows an equilibrium potential of around 1.25 V (Fig. 3f) associated with the dehydrogenation of MgH_2, which is in good agreement with the theoretical value. Meanwhile, the total dehydrogenation capacity amounts to ~1350 mA h g^{-1} (i.e. $MgH_{1.23}$) at this voltage plateau. The kinetic limitations have been eliminated using a GITT mode as the equilibrium status has been reached during the relaxation periods. Therefore, the low Coulombic efficiency (61.4%) indicates a substantial irreversible loss from water splitting. It can also be envisioned that when the charge stage is prolonged (to more than 2200 mA h g^{-1}), regardless of the unavoidable water splitting, the discharge capacity can be further promoted.

Room temperature ionic liquid (RT IL)

It has been proven that both the MTN anode and $Ni(OH)_2$ cathode are chemically stable in the RT IL, [SET3][TFSI], as shown in Fig. S9. Therefore it has been applied as the working electrolyte of the Mg anode based Ni-MH batteries to avoid the passivation issues and the battery structure shows up as MTN ‖ RT IL ‖ $Ni(OH)_2$.

Galvanostatic electrochemical performance (Fig. 4a and b) shows that when the battery is charged to 100 mA h g^{-1} at 5 mA g^{-1}, the voltage undergoes a slopping voltage from 1.5 V to 2.3 V; and the voltage declines from 0.8 V to the cut-off reaching a capacity of 92.4 mA h g^{-1} during discharge. In the second cycle, the overpotential increases during both charge and discharge resulting from an increased electronic resistance induced by the structure change during the first cycle, and the reversible capacity drops to only 53.8 mA h g^{-1}.

To investigate the equilibrium potential, the battery was charged to 100 mA h g^{-1} with a galvanostatic mode at 5 mA g^{-1} and then discharged with a GITT mode, as shown in Fig. 4c. The voltage after relaxation shows a plateau at ~1.0 V, and the overpotential increases with the increasing hydrogen content in the electrode as the electronic conductivity decreases with the increasing concentration of hydrogen in MgH_x. Moreover, the hydrogenation capacity is fully discharged indicating that the low Coulombic efficiency achieved with a galvanostatic discharge mode is due to the limited hydrogen desorption kinetics and electronic conductivity in MgH_x. The equilibrium potential is lower than the nominal value (1.25 V) because of the lower electronic conductivity of [SET3][TFSI] compared to the aqueous alkaline solution and thus a higher ohmic resistance related overpotential.

Considering the high overpotential observed in the galvanostatic voltage profile, the main limitation of the RT IL as a working electrolyte for Ni-MH batteries would be its high proton transfer resistance which results in a high overpotential in dis-/charge. The limited hydrogen desorption kinetics also appears to be a major issue. The discharge capacity can be expected to improve upon further hydrogenation and slow discharge, however, the overpotential will grow as the amount of insulating MgH_2 increases.

High temperature ionic liquid (HT IL)

To accelerate the hydrogen sorption kinetics in MgH_2, molten KOH/NaOH electrolyte was introduced in the MgH_2 based Ni-MH battery working at an elevated temperature of 200 °C. MTN ‖ HT IL ‖ $Ni(OH)_2$ represents the final battery construction.

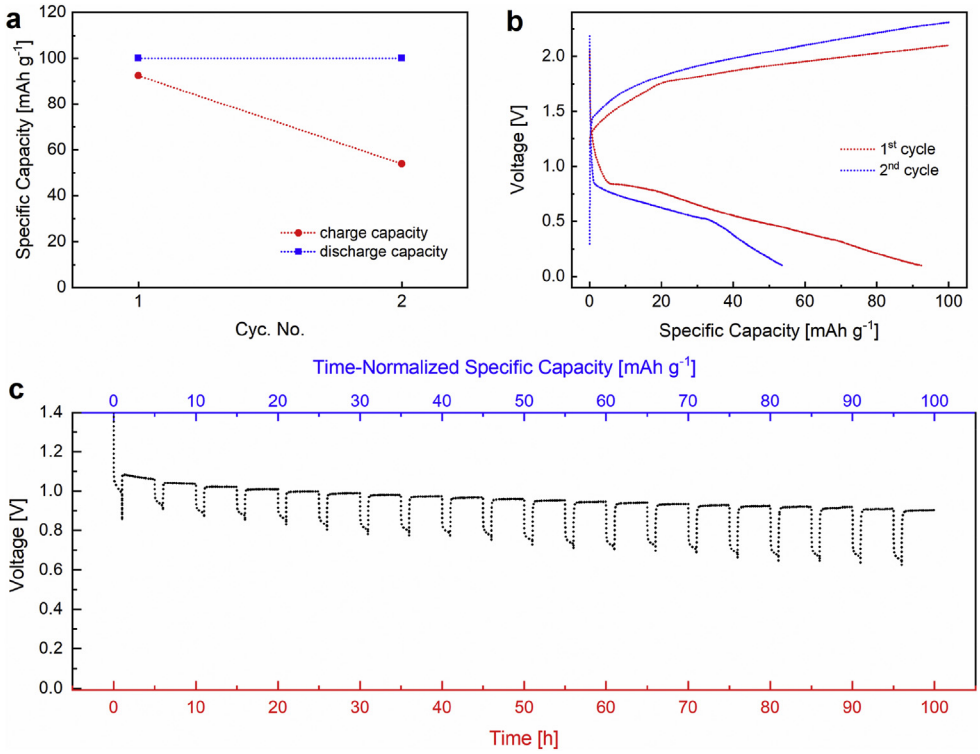

Fig. 4 – Electrochemical performance of a MTN || RT IL || $Ni(OH)_2$ battery working at RT (mass loading of Mg: 7.0 mg cm^{-2}). The charge process was terminated with a target capacity of 100 mA h g^{-1}, while a cut-off voltage of 0.1 V was used for discharge. In (a)–(b), the current densities used for charge and discharge are 5 and 2 mA g^{-1}, respectively. Panel (c) show the GITT discharge voltage profile: discharge at 5 mA g^{-1} for 1 h followed with a rest period of 4 h. The x-axis is scaled in time [h] as well as in the time-normalized specific capacity [mA h g^{-1}]. The battery was charged to a capacity of 100 mA h g^{-1} at 5 mA g^{-1} before it was discharged with a GITT mode.

Fig. 5a shows that, charging the battery to 400 mA h g^{-1} at 20 mA g^{-1}, the discharge capacity reaches ~310 mA h g^{-1}. The limited coulombic efficiency probably results from several factors: a high discharge overpotential due to the low electronic conductivity of the charged electrode, the large distance of hydrogen and electron diffusion through the active material solid and the kinetic barriers for hydrogen release from MgH_2. As a result, a rapid voltage collapse to the cut-off value happens and only a limited capacity is achieved within the working voltage range (Fig. 5b)

To reduce the overpotential, an innovated electrode was fabricated by mechanically compressing the pre-mixed MTN and KOH/NaOH powder (MTN : KOH/NaOH = 1 : 3 in mass) within a commercial nickel foam. The conducting nickel foam provides more electronic conduction throughout the electrode. The presence and homogeneous distribution of KOH/NaOH next to MTN provides a shortened pathway for hydrogen diffusion between the active materials and the electrolyte, largely facilitating the hydrogen transport throughout the electrode. Fig. 5c shows that the Coulombic efficiency has been remarkable, and the discharge overpotential has been reduced showing a main voltage plateau at ~0.45 V related to the hydrogen dissociation from MgH_2 (Fig. 5d).

Interestingly, as shown in the galvanostatic voltage profiles, the working voltage appears to be lower than the nominal value. This can be explained by the cell potential dependence on the temperature determined by Nernst equation which illustrates that the cell voltage declines when the temperature goes up. Moreover, it is noted that the $Ni(OH)_2$/NiOOH system suffers from a low thermal stability at the working temperature, at which $Ni(OH)_2$/NiOOH decomposes (**Reaction (S2) – (S4)**) [61–63], which has been confirmed with XRD (Fig. S10). Based on these observations, we believe that the $Ni(OH)_2$ cathode may have been decomposed into NiO and $NiO{\cdot}(OH)_x$. Thereby the half-cell reactions on the cathode side may be described as **Reaction** (5), (6), which would also lead to a lower working potential.

$$NiO + OH^- = NiOOH + e^- \quad (5)$$

$$NiO{\cdot}(OH)_x + (1-x)\ OH^- = NiOOH + (1-x)\ e^-,\ (0 \le x \le 1) \quad (6)$$

In addition, the slow hydrogen desorption kinetics induces a high overpotential and contributes to the voltage drop as well. The kinetic issues become critical at a higher cycling current rate (50 mA g^{-1}), at which the proton release cannot match the intensive electron flow (Fig. S12).

The charge voltage profiles generally consist of three regions. The main voltage plateau at ~1.2 V is undoubtedly associated with coexistence of α-MgH_x and β- MgH_2 upon the hydrogen absorption in Mg. The short voltage slope before reaching the main voltage plateau can be allocated to the formation of solid solution α-MgH_2. It has been reported that

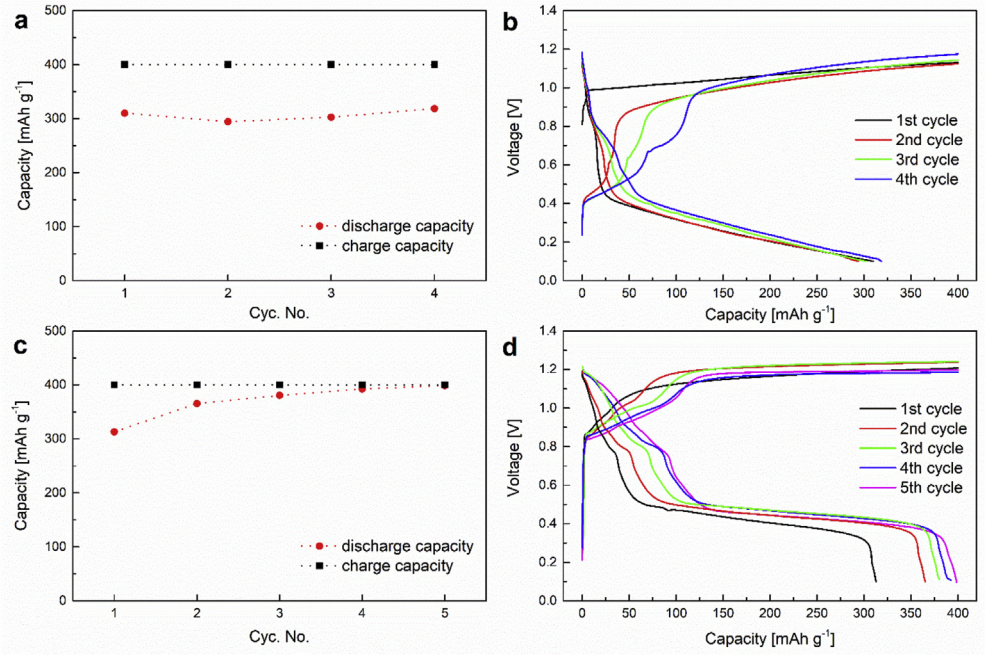

Fig. 5 – Electrochemical performance of the MTN || HT IL || $Ni(OH)_2$ battery cycling at 20 mA g^{-1} working at 200 °C. The charge stage was terminated when the target capacity of 400 mA h g^{-1} was reached and the discharge was stopped with a cut-off voltage of 0.1 V. In (a)–(b), the anode is a pressed pellet of MTN (mass loading of Mg: 4.5 mg cm^{-2}). In (c)–(d), the anode configuration is MTN mixed with KOH/NaOH (MTN : KOH/NaOH = 1 : 3 in mass; mass loading of Mg: 1.9 mg cm^{-2}) mechanically compressed within a commercial nickel foam.

the hydrogenation of Ti occurs at a lower potential range compared to Mg/MgH_2 [28], and therefore the lowest voltage plateau originates from the hydrogenation of TiH_x (formed in **Reaction** (4)). This is also confirmed by comparing the voltage profile of a battery without TiF_3 (Fig. S13). The reverse course takes place during discharge correspondingly.

In addition, it can be anticipated that the charge capacity can simply be improved by extending the charge stage, and the discharge capacity can also be promoted accordingly. However, the lower working potential (i.e. low power output), high overpotential between charge and discharge (i.e. low energy efficiency), and limited hydrogen desorption kinetics (i.e. slow discharge) impose challenges upon its practical applications, which still requires significant efforts for improvement.

Anhydrous alkaline polymer electrolyte

In this work, the alkaline polymer electrolyte based Ni-MH batteries is in a configuration of MTN || PVA-NaOH/KOH || $Ni(OH)_2$. The completely dried PVA-KOH/NaOH membrane exhibits an extremely low ionic conductivity (~2×10^{-7} S cm^{-1} at RT) studied by electrochemical impedance spectroscopy (EIS) (Fig. S15). As a result, the battery exhibited great overpotentials, especially during discharge. The reversible capacity was poor at room temperature because of the immense overpotential and thus rapid voltage drop to the cut-off voltage. Details of the polymer electrolyte based Ni-MH batteries are described in the SI.

It is worth to mention that the charge transfer resistance of the alkaline polymer membrane augments drastically once it is dehydrated due to the high energy barrier for hydroxides to move around the polymer macromolecules. The low ionic conductivity of the anhydrous alkaline polymer electrolyte appears to be a critical issue for its application in Ni-MH batteries, and the proton transfer capability has to be significantly enhanced to ameliorate the battery performance.

Comparison between the battery systems

Table S3 provides a comprehensive comparison between the four types of Ni-MH battery systems investigated in this work. In general, reversible electrochemical proton storage in non-alloyed but catalyzed Mg electrode has been achieved, though the full-cell cycling performance is rather limited.

Ni-MH battery with the alkaline polymer electrolyte achieves a negligible capacity (up to 3.9 mA h g^{-1}) and efficiencies (<10%), due to its extremely low proton conductivity that resulted in great overpotentials. The RT IL based batteries show a moderate capacity as well as Coulombic efficiency, but its low energy efficiency, poor proton conductivity and high cost remain tremendously challenging. The HT IL based batteries achieve the highest reversible capacity (398.8 mA h g^{-1}) and outstanding Coulombic efficiency (99.7%). However, the low discharge voltage and the demanding working conditions (HT and need for protection from high corrosivity) largely compromise its promise for commercial use.

In comparison, alkaline aqueous electrolyte achieves the highest output voltage (1.14 V) and the best energy efficiency (62.3%), which are much superior to the other three. However, such energy efficiency is still to be largely improved for

practical applications. Further improvement will require significantly accelerating the hydrogen sorption kinetics, especially during discharge (hydrogen desorption), and to suppressing the undesired water-splitting issue when charging batteries with a galvanostatic mode.

Conclusions

This work presents a novel Ni-MH battery anode based on TiF_3 catalyzed Mg nanoparticles. Full-cell Ni-MH batteries using commercial $Ni(OH)_2$ cathode and the Mg–TiF_3 anode have been fabricated utilizing several approaches to prevent the surface passivation of Mg from the aggressive aqueous electrolytes. To the best of our knowledge, this is the first time a non-alloy Mg anode has been used for Ni-MH batteries. Reversible electrochemical performance has been observed although the cycling performance is yet to be improved for practical applications. Still the elevated temperature behavior using the HT IL shows the most reversible capacity. We believe that this study will stimulate considerable following research on Mg based anode for Ni-MH batteries.

Declaration of competing interest

The authors declare that they have no known competing financial interests or personal relationships that could have appeared to influence the work reported in this paper.

Acknowledgement

We thank Dr. Anna Glazer-Grzech for help with the initial part of this work. We also thank M. Sc. Yangqun Wu for helping with the experiments using IL electrolytes during her Master thesis project at TU Delft. We also acknowledge financial support from the "A Green Deal in Energy Materials" (ADEM) program funded by Dutch Ministry of Economic Affairs and ADEM industrial partners.

Appendix A. Supplementary data

Supplementary data to this article can be found online at https://doi.org/10.1016/j.ijhydene.2021.03.073.

REFERENCES

[1] Fetcenko MA, Ovshinsky SR, Reichman B, Young K, Fierro C, Koch J, et al. Recent advances in NiMH battery technology. J Power Sources 2007;165:544–51.
[2] Notten PHL, Latroche M. Secondary batteries – NICKEL SYSTEMS | nickel–metal hydride: metal hydrides. In: Garche Jürgen, editor. Encyclopedia of electrochemical power sources. Amsterdam: Elsevier; 2009. p. 502–21.
[3] Young K, Fierro C, Fetcenko MA. Status of Ni/MH battery research and industry. 2011. IEEE Pow Ener Soc Ge; 2011. p. 1–3.
[4] Senoh H, Morimoto K, Inoue H, Iwakura C, Notten PHL. Relationship between equilibrium hydrogen pressure and exchange current for the hydrogen electrode reaction at $MmNi_{(3.9-x)}Mn_{(0.4)}Al_{(x)}Co_{(0.7)}$ alloy electrodes. J Electrochem Soc 2000;147:2451–5.
[5] Nitta N, Wu F, Lee JT, Yushin G. Li-ion battery materials: present and future. Mater Today 2015;18:252–64.
[6] Deng D. Li-ion batteries: basics, progress, and challenges. Energy Sci Eng 2015;3:385–418.
[7] El Kharbachi A, Zavorotynska O, Latroche M, Cuevas F, Yartys V, Fichtner M. Exploits, advances and challenges benefiting beyond Li-ion battery technologies. J Alloys Compd 2020;817:153261.
[8] El Kharbachi A, Dematteis EM, Shinzato K, Stevenson SC, Bannenberg LJ, Heere M, et al. Metal hydrides and related materials. Energy carriers for novel hydrogen and electrochemical storage. J Phys Chem C 2020;124:7599–607.
[9] Hirscher M, Yartys VA, Baricco M, Bellosta von Colbe J, Blanchard D, Bowman RC, et al. Materials for hydrogen-based energy storage – past, recent progress and future outlook. J Alloys Compd 2020;827:153548.
[10] Yartys VA, Lototskyy MV, Akiba E, Albert R, Antonov VE, Ares JR, et al. Magnesium based materials for hydrogen based energy storage: past, present and future. Int J Hydrogen Energy 2019;44:7809–59.
[11] Zhao X, Ma L. Recent progress in hydrogen storage alloys for nickel/metal hydride secondary batteries. Int J Hydrogen Energy 2009;34:4788–96.
[12] Young K-h, Nei J. The current status of hydrogen storage alloy development for electrochemical applications. Materials 2013;6:4574–608.
[13] Santos SF, Nikkuni FR, Ticianelli EA. Magnesium alloys as anode materials for Ni-MH batteries: challenges and opportunities for nanotechnology. In: de Souza FL, Leite ER, editors. Nanoenergy: nanotechnology applied for energy production. Berlin, Heidelberg: Springer Berlin Heidelberg; 2013. p. 179–200.
[14] Ouyang L, Liu F, Wang H, Liu J, Yang X-S, Sun L, et al. Magnesium-based hydrogen storage compounds: a review. J Alloys Compd 2020;832:154865.
[15] Tian Q-F, Zhang Y, Chu H-L, Sun L-X, Xu F, Tan Z-C, et al. The electrochemical performances of $Mg_{0.9}Ti_{0.1}Ni_{1-x}Pd_x$ (x=0–0.15) hydrogen storage electrode alloys. J Power Sources 2006;159:155–8.
[16] Han S-C, Lee PS, Lee J-Y, Züttel A, Schlapbach L. Effects of Ti on the cycle life of amorphous MgNi-based alloy prepared by ball milling. J Alloys Compd 2000;306:219–26.
[17] Zhang Y-h, Wei X, Gao J-l, Hu F, Qi Y, Zhao D-l. Electrochemical hydrogen storage behaviors of as-milled Mg–Ti–Ni–Co–Al-based alloys applied to Ni-MH battery. Electrochim Acta 2020;342:136123.
[18] Zhang Y-h, Zhang W, Yuan Z-m, Bu W-g, Qi Y, Guo S-h. Structure and electrochemical hydrogen storage characteristics of nanocrystalline and amorphous MgNi-type alloy synthesized by mechanical milling. J Iron Steel Res Int 2020;27:952–63.
[19] Niessen RAH, Notten PHL. Electrochemical hydrogen storage characteristics of thin film Mg (X, X = Sc, Ti, V, Cr) compounds. Electrochem Solid State Lett 2005;8:A534–8.
[20] Kalisvaart WP, Niessen RAH, Notten PHL. Electrochemical hydrogen storage in MgSc alloys: a comparative study between thin films and bulk materials. J Alloys Compd 2006;417:280–91.
[21] Niessen RAH, Vermeulen P, Notten PHL. The electrochemistry of Pd-coated $Mg_ySc_{(1-y)}$ thin film electrodes: a thermodynamic and kinetic study. Electrochim Acta 2006;51:2427–36.

[22] Du Q, Li S, Huang G, Feng Q. Enhanced electrochemical kinetics of magnesium-based hydrogen storage alloy by mechanical milling with graphite. Int J Hydrogen Energy 2017;42:21871–9.

[23] Rongeat C, Roué L. On the cycle life improvement of amorphous MgNi-based alloy for Ni–MH batteries. J Alloys Compd 2005;404–406:679–81.

[24] Zhang Y, Liao B, Chen L-X, Lei Y-Q, Wang Q-D. The effect of Ni content on the electrochemical and surface characteristics of $Mg_{90-x}Ti_{10}Ni_x$ (x=50, 55, 60) ternary hydrogen storage electrode alloys. J Alloys Compd 2001;327:195–200.

[25] Nikkuni FR, Santos SF, Ticianelli EA. Microstructures and electrochemical properties of $Mg_{49}Ti_6Ni_{(45-x)}M_x$ (M = Pd and Pt) alloy electrodes. Int J Energy Res 2013;37:706–12.

[26] Rongeat C, Grosjean MH, Ruggeri S, Dehmas A, Bourlot S, Marcotte S, et al. Evaluation of different approaches for improving the cycle life of MgNi-based electrodes for Ni-MH batteries. J Power Sources 2006;158:747–53.

[27] Ouyang LZ, Chung CY, Wang H, Zhu M. Microstructure of Mg–Ni thin film prepared by direct current magnetron sputtering and its properties as a negative electrode. J Vac Sci Technol 2003;21:1905–8.

[28] Manivasagam TG, Iliksu M, Danilov DL, Notten PHL. Synthesis and electrochemical properties of binary MgTi and ternary MgTiX (X = Ni, Si) hydrogen storage alloys. Int J Hydrogen Energy 2017;42:23404–15.

[29] Hapçı Ağaoğlu G, Orhan G. Elaboration and electrochemical characterization of Mg–Ni hydrogen storage alloy electrodes for Ni/MH batteries. Int J Hydrogen Energy 2017;42:8098–108.

[30] Chen H, Liang H, Dai W, Lu C, Ding K, Bi J, et al. $MgScH_{15}$: a highly stable cluster for hydrogen storage. Int J Hydrogen Energy 2020;45:32260–8.

[31] Li XD, Elkedim O, Cuevas F, Chassagnon R. Structural and hydrogenation study on the ball milled TiH_2–Mg–Ni. Int J Hydrogen Energy 2015;40:4212–8.

[32] Fadonougbo JO, Kim H-J, Suh B-C, Suh J-Y, Lee Y-S, Shim J-H, et al. Kinetics and thermodynamics of near eutectic Mg-Mg_2Ni composites produced by casting process. Int J Hydrogen Energy 2020;45:29009–22.

[33] Fu Y, Ding Z, Ren S, Li X, Zhou S, Zhang L, et al. Effect of in-situ formed Mg_2Ni/Mg_2NiH_4 compounds on hydrogen storage performance of MgH_2. Int J Hydrogen Energy 2020;45:28154–62.

[34] Zhang Z, Elkedim O, Zhang M, Bassir D. Systematic investigation of mechanically alloyed Ti-Mg-Ni used as negative electrode in Ni-MH battery. J Solid State Electrochem 2018;22:1669–76.

[35] Muthu P, Sinnaeruvadi K. Facilitation of quasi-reversible effect with rapid diffusion kinetics on $Mg_{0.9-x}Ti_{0.1}Ni_x$ high energy ball milled powders for Ni-MH batteries. J Alloys Compd 2019;793:155–69.

[36] Zhang M, Xiao X, Hang Z, Chen M, Wang X, Zhang N, et al. Superior catalysis of NbN nanoparticles with intrinsic multiple valence on reversible hydrogen storage properties of magnesium hydride. Int J Hydrogen Energy 2021;46:814–22.

[37] Barkhordarian G, Klassen T, Bormann R. Catalytic mechanism of transition-metal compounds on Mg hydrogen sorption reaction. J Phys Chem B 2006;110:11020–4.

[38] Jin S-A, Shim J-H, Cho YW, Yi K-W. Dehydrogenation and hydrogenation characteristics of MgH_2 with transition metal fluorides. J Power Sources 2007;172:859–62.

[39] Bhat VV, Rougier A, Aymard L, Darok X, Nazri G, Tarascon JM. Catalytic activity of oxides and halides on hydrogen storage of MgH_2. J Power Sources 2006;159:107–10.

[40] Zhu W, Panda S, Lu C, Ma Z, Khan D, Dong J, et al. Using a self-assembled two-dimensional MXene-based catalyst (2D-Ni@Ti_3C_2) to enhance hydrogen storage properties of MgH_2. ACS Appl Mater Interfaces 2020;12:50333–43.

[41] Mulder FM, Singh S, Bolhuis S, Eijt SWH. Extended solubility limits and nanograin refinement in Ti/Zr fluoride-catalyzed MgH_2. J Phys Chem C 2012;116:2001–12.

[42] Grzech A, Lafont U, Magusin PCMM, Mulder FM. Microscopic study of TiF_3 as hydrogen storage catalyst for MgH_2. J Phys Chem C 2012;116:26027–35.

[43] Xu Y, Mulder FM. TiF_3 catalyzed MgH_2 as a Li/Na ion battery anode. Int J Hydrogen Energy 2018;43:20033–40.

[44] Wu JK. Electrochemical method for studying hydrogen in iron, nickel and palladium. Int J Hydrogen Energy 1992;17:917–21.

[45] Altunoglu AK, Blackburn DA, Braithwaite NSJ, Grant DM. Permeation of hydrogen through nickel foils: surface reaction rates at low temperatures. J Less Common Met 1991;172–174:718–26.

[46] Balducci A. Ionic liquids in lithium-ion batteries. Top Curr Chem 2017;375:20.

[47] Díaz M, Ortiz A, Ortiz I. Progress in the use of ionic liquids as electrolyte membranes in fuel cells. J Membr Sci 2014;469:379–96.

[48] Young K-h, Ng YK, Bendersky AL. A technical report of the robust affordable next generation energy storage system-BASF program. Batteries 2016;2:2.

[49] Matsumoto H, Matsuda T, Miyazaki Y. Room temperature molten salts based on trialkylsulfonium cations and bis(trifluoromethylsulfonyl)imide. Chem Lett 2000;29:1430–1.

[50] Rennie AJR, Martins VL, Torresi RM, Hall PJ. Ionic liquids containing sulfonium cations as electrolytes for electrochemical double layer capacitors. J Phys Chem C 2015;119:23865–74.

[51] Wei D, Ng TW. Application of novel room temperature ionic liquids in flexible supercapacitors. Electrochem Commun 2009;11:1996–9.

[52] Ganley JC. An intermediate-temperature direct ammonia fuel cell with a molten alkaline hydroxide electrolyte. J Power Sources 2008;178:44–7.

[53] Licht S, Cui B, Wang B, Li F-F, Lau J, Liu S. Ammonia synthesis by N_2 and steam electrolysis in molten hydroxide suspensions of nanoscale Fe_2O_3. Science 2014;345:637–40.

[54] Li B, Lu X, Yuan J, Zhu Y, Li L. Alkaline poly(vinyl alcohol)/poly(acrylic acid) polymer electrolyte membrane for Ni-MH battery application. Ionics 2015;21:141–8.

[55] Mohamad AA, Arof AK. Ni-MH battery based on plasticized alkaline solid polymer electrolytes. Ionics 2008;14:415–20.

[56] Mohamad AA, Mohamed NS, Alias Y, Arof AK. Studies of alkaline solid polymer electrolyte and mechanically alloyed polycrystalline Mg_2Ni for use in nickel metal hydride batteries. J Alloys Compd 2002;337:208–13.

[57] Mulder FM, Singh S, Bolhuis S, Eijt SWH. Extended solubility limits and nanograin refinement in Ti/Zr fluoride-catalyzed MgH_2. J Phys Chem C 2012;116:2001–12.

[58] Posey FA, Morozumi T. Theory of potentiostatic and galvanostatic charging of the double layer in porous electrodes. J Electrochem Soc 1966;113:176–84.

[59] Coridan RH, Nielander AC, Francis SA, McDowell MT, Dix V, Chatman SM, et al. Methods for comparing the performance of energy-conversion systems for use in solar fuels and solar electricity generation. Energy Environ Sci 2015;8:2886–901.

[60] Liu YF, Pan HG, Gao MX, Wang QD. Advanced hydrogen storage alloys for Ni/MH rechargeable batteries. J Mater Chem 2011;21:4743–55.
[61] Chen J, Bradhurst DH, Dou SX, Liu HK. Nickel hydroxide as an active material for the positive electrode in rechargeable alkaline batteries. J Electrochem Soc 1999;146:3606–12.
[62] Gu HM, Wang W, Zhai YC. Study on preparation and properties of β-NiOOH. Adv Mater Res 2011;239–242:646–9.
[63] Horányi TS. The thermal stability of the β-$Ni(OH)_2$-β-NiOOH system. Thermochim Acta 1989;137:247–53.